

Optimal control of diffuser shapes for confined turbulent shear flows

G.P. Benham ^{1†}, I.J. Hewitt ¹, C.P. Please ¹, and P. Bird ²

¹Mathematical Institute, University of Oxford, Andrew Wiles Building, Radcliffe Observatory Quarter, Woodstock Road, Oxford OX2 6GG United Kingdom

²VerdErg Renewable Energy Limited, 6 Old London Rd, Kingston upon Thames KT2 6QF, United Kingdom

(Received xx; revised xx; accepted xx)

A model for the development of turbulent shear flows, created by non-uniform parallel flows in a confining channel, is used to identify the diffuser shape that maximises pressure recovery when the inflow is non-uniform. Wide diffuser angles tend to accentuate the non-uniform flow, causing poor pressure recovery. On the other hand, shallow diffuser angles create longer regions with large wall drag, which is also detrimental to pressure recovery. Thus, optimal diffuser shapes strike a balance between the two effects. We use a simple model which describes the evolution of an approximate flow profile and pressure in the diffuser. The model equations form the dynamics of an optimal control problem where the control is the diffuser channel shape. A numerical optimisation approach is used to solve the optimal control problem and we use analytical results to interpret the numerics in some limiting cases. The results of the optimisation are compared to calculations from computational fluid dynamics.

1. Introduction

In this study, we consider a class of expanding channel flows in which the inflow is non-uniform, resulting in turbulent shear layers confined within the channel. Expanding channels, known as diffusers, have the function of converting high-speed low-pressure flow to low-speed high-pressure flow. Diffusers have numerous applications, from turbines in aerospace and hydropower (Simone *et al.* 2012; Chamorro *et al.* 2013; Kang *et al.* 2014) to automotive design (Jones & Smith 2003). There is a large literature on diffusers in the case where the inflow is uniform (see (Blevins 1984)), but a limited literature for non-uniform inlet flows and flows with shear layers (Benham *et al.* 2017).

In the case where the inflow is uniform and there are no shear layers within the flow, diffusers are usually designed to be straight sided, and the expansion angle is critical to performance (Blevins 1984). The optimal angle strikes a balance between not being too shallow, since thin channels have larger wall drag, and not being too wide, since wide expansion angles result in boundary layer separation and poor consequent pressure recovery (Douglas *et al.* 1979). The optimum angle varies slightly, depending on the inflow boundary layer thickness, and whether the diffuser is two-dimensional or axisymmetric.

In the case where the inflow is non-uniform, resulting in shear layers confined within the diffuser, we must account for the additional effect of the channel shape on the development of shear layers and the non-uniform flow profile. An important feature in understanding non-uniform flows is the interplay between changes in the pressure and the kinetic energy flux factor, which is a normalised measure of how non-uniform a flow is.

† Email address for correspondence: benham@maths.ox.ac.uk

A decrease in kinetic energy flux factor corresponds to a more uniform flow, and a rise in pressure. Diffusers with wide angles have the tendency to accentuate non-uniform flows and, in some extreme cases, create a jet-like outflow (Blevins 1984). In such cases, the outflow has a high kinetic energy flux and, hence, a low pressure recovery. On the other hand, diffusers with shallow angles have longer, narrower profiles, which create a lot of wall drag and consequently a larger drop in pressure. Optimal diffuser shapes, therefore, must strike a balance between mixing the flow in a narrow section and then widening the flow to decrease wall drag.

In this paper, we attempt to identify and understand the diffuser shape which satisfies these criteria. In contrast to diffusers with uniform inflow, where the channel shape is only restricted due to boundary layer separation, diffusers with non-uniform inflow have a shape which is also restricted due to the effect of accentuating the non-uniform flow. We find that in some cases, the optimum diffuser angle for non-uniform flow is smaller than typically used for diffusers with uniform inflow. Therefore, from a design perspective, the effect of the inflow profile cannot be ignored. In our analysis, we show how to optimise diffuser design based on the nature of the non-uniform inflow.

The development of the non-uniform flow profile, which is fundamental to pressure recovery, can be described using a simple model for turbulent shear layers in confining channels (Benham *et al.* 2017). The model predictions have good agreement with CFD and experimental work for a range of channel shapes and Reynolds numbers. The model constitutes a differential-algebraic system of equations which governs the continuous dependence of the flow profile and pressure on the diffuser shape. It assumes that the flow is composed of plug regions separated by a linear shear layer. We find that the change in dynamics when the shear layer reaches the channel walls plays an important role in the optimal control.

It has been shown that, using this model to investigate pressure recovery of a simple class of diffuser shapes, an optimum can be found by exhaustively searching the design space (Benham *et al.* 2017). However, when we do not make such restrictions and treat the diffuser shape as a continuous control, it is necessary to seek more complex tools to solve the problem. In this paper, we use the model as the basis for numerical optimisation of the diffuser shape, where the governing equations form the optimisation constraints. Such problems, as well as PDE-constrained optimisation problems, often arise in the field of flow control. With the advancement of computational power, these problems have become more feasible to solve. There are many different approaches to solving such problems which are discussed by Gunzburger (2002).

In our approach we exploit the fact that the model is one-dimensional and, upon discretisation, there is a relatively low number of degrees of freedom. This, in combination with the use of automatic differentiation to calculate gradients, allows us to perform gradient-descent optimisation with relatively low computational effort (Nocedal & Wright 2006). In certain limiting cases, we solve the optimal control problem analytically using Pontryagin's maximum principle (Pontryagin 1987) and use these solutions to aid interpretation of the results from the numerical optimisation. CFD calculations, using a $k - \epsilon$ turbulence model (Lauder & Spalding 1974), are compared with the optimal solutions found using the simple model.

Section 2 outlines the model for the development of shear layers in confining channels, and sets up the optimal control problem, discussing the choice of objective, the constraints and the number of parameters. Section 3 outlines a numerical method for solving the optimal control problem and, using this method, we investigate optimal diffuser shapes in several different cases. In section 4 we find analytical solutions to the optimal control problem in two of these cases. In section 5, we present some CFD calculations and

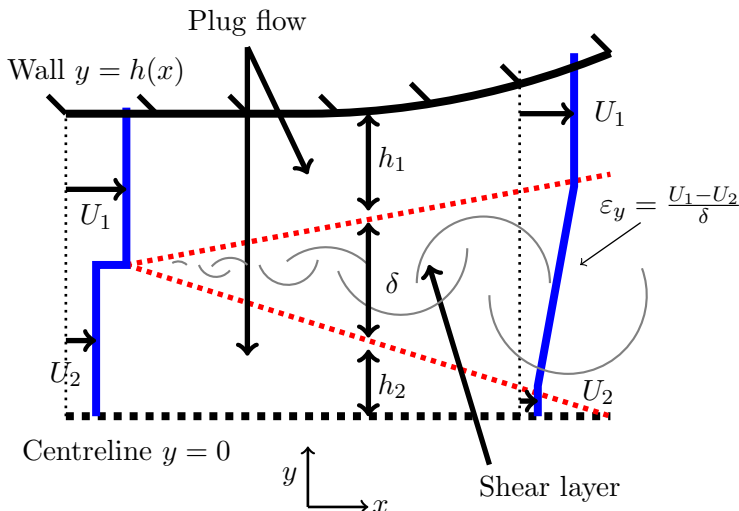


Figure 1: Schematic diagram of symmetric flow in a half channel. We model the flow as plug flow regions separated by a linear turbulent shear layer. The model governs a reduced number of variables U_1 , U_2 , h_1 , h_2 , δ , ε_y and p , which are all functions of x . The aspect ratio is exaggerated.

compare them to results of the optimisation. Section 6 summarises the results of the paper and discusses the dependance of the optimal shapes on the set of parameters.

2. The model and optimal control problem

2.1. Modelling turbulent shear layers in confining channels

We start by outlining the simple model for the development of turbulent shear layers in confining channels. A more detailed description of the model, including a derivation of the governing equations, is given by Benham *et al.* (2017). We focus our attention on a class of symmetric channel flows where the inflow is composed of a slower moving central stream with speed U_2 and a faster outer stream with speed U_1 . Initially we consider two-dimensional flow in a half channel $0 < y < h(x)$. Later, we extend the model to the axisymmetric case.

A turbulent shear layer forms at the place where the parallel streams meet. We approximate the flow profile by decomposing it into two plug regions separated by a shear layer in which the velocity varies linearly between U_1 and U_2 (see figure 1). The approximate velocity profile is

$$u(x, y) = \begin{cases} U_2(x) & : 0 < y < h_2(x), \\ U_2(x) + \varepsilon_y(x)(y - h_2(x)) & : h_2(x) < y < h(x) - h_1(x), \\ U_1(x) & : h(x) - h_1(x) < y < h(x), \end{cases} \quad (2.1)$$

where h_1 and h_2 are the widths of the two plug regions, $\delta = h - h_1 - h_2$ is the width of the shear layer, and $\varepsilon_y = (U_1 - U_2)/\delta$ is the shear rate. As the shear layer grows with x , the shear rate decays (Schlichting *et al.* 1960). We assume that the shear rate decays according to,

$$\frac{U_1 + U_2}{2} \frac{d\varepsilon_y}{dx} = -S\varepsilon_y^2, \quad (2.2)$$

where S is a non-dimensional spreading parameter which we have determined as $S = 0.11$ for two-dimensional shear layers (Benham *et al.* 2017). Equation (2.2) can be derived from an entrainment argument (see appendix in (Benham *et al.* 2017)), or by analogy with the growth of free shear layers. Assuming that the channel is long and thin, boundary layer theory (Schlichting *et al.* 1960) indicates that, to good approximation, the pressure does not vary across the channel width $p = p(x)$. Averaged across the channel, conservation of mass and momentum equations are

$$\int_0^h \rho u dy = Q, \quad (2.3)$$

$$\frac{d}{dx} \left(\int_0^h \rho u^2 dy \right) + h \frac{dp}{dx} = \tau_w, \quad (2.4)$$

where ρ is the density, Q is the constant mass flux (per unit depth), and τ_w is the wall shear stress. We model τ_w using the Darcy-Weisbach equation

$$\tau_w = -\frac{1}{8} f \rho U_1^2, \quad (2.5)$$

where f is the empirical Darcy friction factor. Finally, we ignore viscous dissipation in the plug flow regions, since it is small compared to that at the walls and in the shear layer. Hence, in the plug regions, we assume Bernoulli's equation holds (Batchelor 2000). In certain cases, especially when the diffuser angle is wide, the speed of the slower plug region U_2 may decrease and reach zero. This has been observed in CFD simulations, which we display in Appendix A. In such cases there is a portion of recirculating flow in the central part of the diffuser. We do not resolve the recirculation in these regions but since velocities are small, as observed in CFD, we treat the regions as stagnant zones with zero velocity. Bernoulli's equation in each plug region is implemented in a complementarity format for convenience

$$h_1 \left(p - p(0) + \frac{1}{2} \rho (U_1^2 - U_1(0)^2) \right) = 0, \quad \text{and} \quad h_1 \geq 0, \quad (2.6)$$

$$U_2 h_2 \left(p - p(0) + \frac{1}{2} \rho (U_2^2 - U_2(0)^2) \right) = 0, \quad \text{and} \quad h_2 \geq 0, \quad U_2 \geq 0. \quad (2.7)$$

The complementarity format of equations (2.6) and (2.7) ensures that when either of the plug regions disappears, or if the slower plug region stagnates, Bernoulli's equation ceases to hold in that region. We find good comparison between our model predictions of the stagnant region and CFD calculations, which we discuss in Appendix A.

To summarise, the simple model describes the evolution of the non-uniform velocity profile $u(x, y)$, given by (2.1), and pressure $p(x)$ in a confining channel $y = h(x)$. Equations (2.2) - (2.7) govern the variables U_1 , U_2 , h_1 , h_2 , δ , ε_y and p , which are all functions of x . These equations can be solved for all x given inflow conditions at $x = 0$. For almost all of this manuscript, we shall only consider situations in which the shear layer forms at $x = 0$, such that $\delta(0) = 0$ and $\varepsilon_y(0) = \infty$. In one example called the “pure shear limit” we consider a purely sheared inflow with $\delta(0) = h(0)$. Pressure is measured with reference to the value at the inlet so we can take $p(0) = 0$ without loss of generality. All other inflow conditions form part of the set of parameters which we discuss in 2.2.

We can extend the model to account for axisymmetric flows simply. For axisymmetric flow in a cylindrical channel $0 \leq r \leq h$, we assume that the velocity profile is identical to equation (2.1) except with y replaced with r . In the axisymmetric version of the model, equations (2.2), (2.5) and (2.6)-(2.7) remain unchanged, but equations (2.3)

and (2.4) are altered to account for radial symmetry

$$2\pi \int_0^h \rho u r dr = Q, \quad (2.8)$$

$$2\pi \frac{d}{dx} \left(\int_0^h \rho u^2 r dr \right) + \pi h^2 \frac{dp}{dx} = 2\pi h \tau_w. \quad (2.9)$$

The results of the axisymmetric and two-dimensional cases are compared in section 3.

2.2. Formulation of the optimal control problem

Diffuser performance can be measured in a number of different ways, for example using a pressure recovery coefficient or a loss coefficient (Blevins 1984). The pressure recovery coefficient C_p is a measure of the pressure gain in the diffuser from inlet to outlet, relative to the kinetic energy flux at the inlet. The loss coefficient K_l is a measure of the total energy lost from inlet to outlet, relative to the kinetic energy flux at the inlet. For the optimal control problem, we could choose either of these coefficients as the objective. Maximising C_p , for a given inflow, would produce the diffuser that converts the greatest amount of inflow kinetic energy into static pressure at the outflow. Minimising K_l , for a given inflow, would produce the diffuser with the maximum amount of energy at the outflow.

For this paper, we choose the pressure recovery coefficient as the objective. There are several ways to define the coefficient, but we shall use the so-called “mass-averaged” pressure recovery (Filipenco *et al.* 1998), which is defined as

$$C_p = \frac{\int_0^h u p dy|_{x=L} - \int_0^h u p dy|_{x=0}}{\int_0^h \frac{1}{2} \rho u^3 dy|_{x=0}}, \quad (2.10)$$

for the two-dimensional case and

$$C_p = \frac{\int_0^h u p r dr|_{x=L} - \int_0^h u p r dr|_{x=0}}{\int_0^h \frac{1}{2} \rho u^3 r dr|_{x=0}}, \quad (2.11)$$

for the axisymmetric case. The pressure recovery coefficient can take values $C_p \in [-\infty, 1]$, where $C_p = 1$ when all the kinetic energy of the inlet flow is converted into static pressure. For a given area ratio $h(L)/h(0)$ and inflow, there is a maximum possible pressure recovery $C_{p_I} \leq 1$ (Blevins 1984). For uniform inviscid flow this ideal limit is $C_{p_I} = 1 - (h(0)/h(L))^2$, but for non-uniform flow it is not known what the limit is.

Now that we have chosen a suitable objective for the optimisation, we need to define a control. The diffuser shape is ultimately the control of the problem, but there are several different ways to formulate it. For example, we could use the shape function $h(x)$ as the control, or we could use its derivative, or even the second derivative. To aid our choice of control, we consider the regularity requirements of the final shape. If the minimum requirement is that the shape be continuous, it will be convenient to choose the derivative of h as the control. If we also require smoothness (i.e. existence of the first derivative of h), then it will be convenient to choose the second derivative of h as the control. However, if no such requirements exist, then it is satisfactory to use h itself as the control. For this paper, we restrict ourselves to continuous but non-smooth shapes, and so we choose the shape derivative, or diffuser angle,

$$\alpha(x) = \frac{dh}{dx}, \quad (2.12)$$

as the control for optimising the diffuser shape. An additional possible control of the problem is the channel length L . For now, we consider this fixed, but later we discuss the possibility of including L as a free parameter.

After defining both the objective and the control of the optimisation, we now discuss the constraints. The most obvious constraints on the variables are the governing equations and inflow conditions. In addition, we may also want some constraints on the outflow. As mentioned earlier, constraining $h(L)/h(0)$ gives us a fixed maximum value for the pressure recovery. If $h(L)/h(0)$ is unconstrained, then the pressure recovery will be maximised with $h(L)/h(0) = \infty$ (Blevins 1984). However, this is impractical for construction and, due to Bernoulli's equation, we see that pressure recovery decays rapidly with h (like $\sim 1/h^2$ for two-dimensional flows and like $\sim 1/h^4$ for axisymmetric flows) so that a large majority of pressure is recovered for relatively small values of $h(L)/h(0)$. For example, if $h(L)/h(0) = 3$ in uniform inviscid axisymmetric flow, the pressure recovery is $C_p \approx 0.99$. Therefore, for practical considerations, we constrain the channel width at the outflow

$$h(L) = h_L. \quad (2.13)$$

Another important constraint we need to consider is the boundedness of the control α . In particular, we note that for large values of the diffuser angle, boundary layers at the channel walls have the tendency to separate (Douglas *et al.* 1979). This phenomenon, which is often called ‘diffuser stall’, is not something that we attempt to capture with our model. However, it is known that diffuser stall has a detrimental effect on pressure recovery (because the outflow is jet-like and, therefore, has a large kinetic energy flux). Considering this, we give the control α an upper bound corresponding to the smallest diffuser angle which causes stall. The first appreciable stall of a straight walled diffuser is at $\alpha \approx \tan 7^\circ$ for the two-dimensional case and $\alpha \approx \tan 3.5^\circ$ for axisymmetric diffusers (Blevins 1984). Furthermore, due to engineering constraints, it might not always be possible to construct channel shapes which contract more than a certain angle. Therefore, a lower bound on the control may also be necessary. If we denote the upper and lower bounds α_{max} and α_{min} , respectively, then α satisfies the box constraints

$$\alpha_{min} \leq \alpha \leq \alpha_{max}. \quad (2.14)$$

It should be noted that, whilst equation (2.14) applies, the optimal control might not necessarily attain these bounding values. In such cases, equation (2.14) may be considered irrelevant.

To summarise the formulation of the optimal control problem, we seek to maximise the pressure recovery by manipulating the control $\alpha(x)$ within its bounds:

$$\max_{\alpha_{min} \leq \alpha(x) \leq \alpha_{max}} C_p, \quad (2.15)$$

with the constraints that equations (2.2)-(2.7) hold, together with inlet conditions for all variables at $x = 0$, and the end constraint (2.13).

Before solving the optimal control problem, we note that there are several parameters which affect the solution. We list these parameters in table 1 and discuss them in more detail in section 6.

3. Numerical optimisation

We solve the optimisation problem (2.15) numerically by discretising the variables U_1 , U_2 , h_1 , h_2 , δ , ε_y and p , and treating each discretised value as a degree of freedom. We use the interior point method (Nocedal & Wright 2006) (with the IpOpt library (Wächter &

$U_2(0)/U_1(0)$	Velocity ratio
$h_2(0)/h(0)$	Plug width ratio
$h(L)/h(0)$	Expansion ratio
$L/h(0)$	Length ratio
$\alpha_{min}, \alpha_{max}$	Minimum/maximum angle
S	Spreading parameter
f	Darcy friction factor

Table 1: List of the parameters of the optimal control problem. We treat the first 5 of these parameters as problem-specific, whereas the last 2 parameters are considered fixed. We also make use of the shorthand $h_0 = h(0)$ and $U_0 = U_1(0)$.

Biegler 2006)) for non-linear constrained optimisation problems. Gradients are calculated using automatic differentiation in the the JuMP package (Dunning *et al.* 2017) of the Julia programming language (Bezanson *et al.* 2017). The equality constraints we need to impose are equations (2.2)-(2.7), inlet conditions and the terminal condition (2.13). There are also the inequality constraints (2.14) and those listed in the complementarity condition (2.6)-(2.7). As is often done, we impose the equality constraints using the quadratic penalty method (Nocedal & Wright 2006), where we subtract their residual squared from the objective. For example, if our objective is to maximise the function $g(x)$ subject to the equality constraint $c(x) = 0$, then we replace the objective with

$$\max g(x) - \mu c(x)^2, \quad (3.1)$$

where μ is a penalty parameter. Our inequality constraints are simple box constraints. These are dealt with by the interior point method using logarithmic barrier functions. More details, including how to choose the penalty parameter μ and barrier functions, are discussed by Nocedal & Wright (2006).

It is not known whether this optimisation problem is convex so, assuming it is non-convex, there may exist multiple solutions. In order to ensure that we are confident about the optimal solutions that are found, we use many different initial guesses to initialise the interior point method (although we have not yet found multiple solutions).

The governing equations of the model consist of the algebraic equations, which are (2.1)-(2.3), (2.5)-(2.7) and inflow conditions, and the differential equations which are (2.2), and (2.4). We discretise the variables into n points and impose the algebraic equations exactly at every point. The differential equations are imposed using a second order central finite difference scheme. It should be noted that whilst the complementarity conditions enforce a switch in the governing equations and may produce non-smooth behaviour in the solution, the equations themselves are smooth and can therefore be differentiated. Computation time is fast, owing to the use of automatic differentiation to calculate gradients. With 8 variables $U_1, U_2, h_1, h_2, \delta, \varepsilon_y, p, h$ and one control α , the total number of degrees of freedom is $9n$. For a discretisation of $n = 500$ grid points, and therefore 4500 degrees of freedom, computation time is of the order of one minute on a laptop computer.

3.1. Results of the numerical optimisation

Having briefly discussed the optimisation routine, we use it to optimise channel shapes in several different cases. In each case, we maintain all variables in non-dimensional form with reference to typical length scales and velocity scales. We use the initial channel width as a typical length scale $h_0 = h(0)$ and the speed of the faster plug region at the inlet

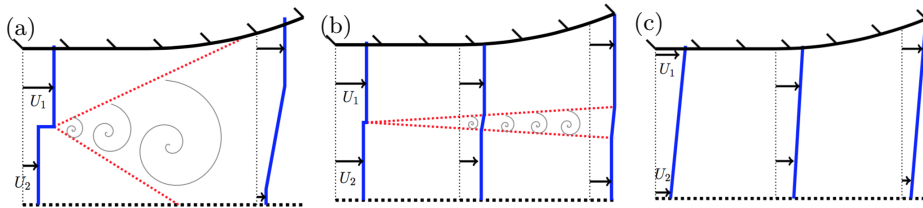


Figure 2: Schematic diagram of the different cases. a) General case, where L is sufficiently large such that the shear layers reach across the channel. b) “Small shear limit” case, when $U_2(0)/U_1(0) \approx 1$ such that the shear layer never reaches across the channel. c) “Pure shear limit”, where the shear layer has already spread across the channel such that there are no plug regions of flow.

as a typical velocity scale $U_0 = U_1(0)$. We choose three case studies to optimise, which are illustrated in figure 2. In the first case, which is illustrated in figure 2 (a), we look at two-dimensional flow and choose parameter values $U_2(0)/U_0 = 0.3$, $h_2(0)/h_0 = 0.5$, $h(L)/h_0 = 1.5$, $L/h_0 = 30$, $\alpha_{min} = 0^\circ$ and $\alpha_{max} = \tan 7^\circ$. The other parameters are taken as $S = 0.11$ and $f = 0.01$ (which corresponds to a Reynolds number of $Re = 10^6$ and hydraulically smooth walls (McKeon *et al.* 2005)). The number of grid points is $n = 100$. Simultaneously, we also investigate axisymmetric flow with the same parameter values, except with $\alpha_{max} = \tan 3.5^\circ$ (this is the smallest angle for cylindrical diffuser stall). We plot the optimal shape and corresponding velocity colour map for the two-dimensional case in figure 3 (a) and pressure plot in figure 3 (e). The axisymmetric case is plotted in figure 3 (b) and 3 (f).

In both cases, the optimal shape is approximately divided into a straight part, followed by a widening part, followed by another straight part. The length of the first straight section aligns with the length it takes for the shear layer to spread completely across the channel. This suggests that mixing the flow to a more uniform profile is advantageous for the widening part to perform well. This is as expected because, as mentioned earlier, diffusers tend to accentuate non-uniform flow, producing an outflow with large kinetic energy flux (and therefore a low pressure recovery). However, as discussed earlier, long thin channels cause large loss in pressure due to wall drag. Therefore, the optimal shape must have a straight section which is sufficiently long that the shear layer reaches across the channel, making the flow more well mixed, but no longer than that because of wall drag.

Interestingly, the widening part of the channel widens at a shallower angle than the maximum value (around $\tan 2.3^\circ$ compared to $\tan 7^\circ$). So the upper bound on α is not needed in this case. This behaviour is unexpected since diffusers are usually designed with a widening angle as close to $\tan 7^\circ$ as possible, regardless of the inflow. These results suggest that there is an optimum widening angle which is determined by the non-uniform inflow, rather than the risk of boundary layer separation.

Because the optimal diffuser shape naturally splits into three sections, we also try restricting the control α in this way to see if we can attain a near optimal solution with a piecewise linear shape. We parameterise α by splitting it into three parts: a straight part with $\alpha = 0$ for $0 \leq x < x_1$; a widening part with constant $\alpha > 0$ for $x_1 \leq x < x_2$, and a final straight part with $\alpha = 0$ for $x_2 \leq x \leq L$. We treat x_1 and x_2 as control parameters and the value of α in the middle section is determined by the condition

$$\alpha = \frac{h_L - h_0}{x_1 - x_2} \quad (3.2)$$

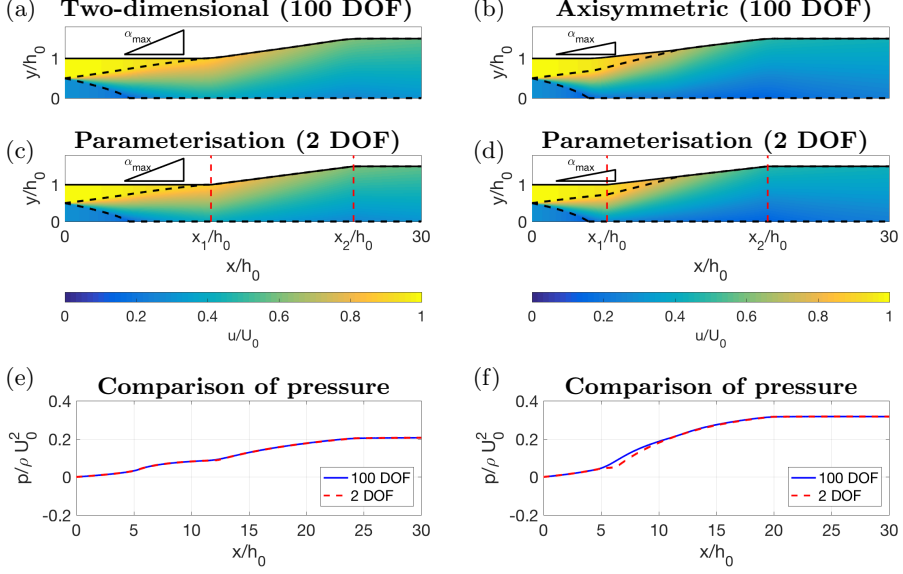


Figure 3: Optimal diffuser shape in the two-dimensional case (a, c, e) and the axisymmetric case (b, d, f), displaying velocity colour maps and pressure plots. The inflow has $U_2(0)/U_0 = 0.3$ and $h_2(0)/h_0 = 0.5$, the expansion ratio is $h(L)/h_0 = 1.5$ and the length ratio is $L/h_0 = 30$. The lower limit for the diffuser angle in both cases is $\alpha_{min} = 0^\circ$. The upper limit is $\alpha_{max} = \tan 7^\circ$ for the two-dimensional case and $\tan 3.5^\circ$ for the axisymmetric case.

We optimise pressure recovery, using the same algorithm as before, but with α having only 2 degrees of freedom (DOF), the two parameters x_1 and x_2 . We plot the optimal diffuser shape and velocity plot in figure 3 (c), which is near identical to that obtained with 100 DOF. Moreover, the pressure plot displayed in figure 3 (e) shows a very close match. The pressure recovery coefficient for 2 DOF is $C_p = 0.5203$ compared to $C_p = 0.5205$ for 100 DOF, suggesting that piecewise linear diffuser shapes are a very good approximation in this case. In figure 4 (a) we plot the optimal control next to that obtained with 100 DOF and they exhibit a close match. Below, in figure 4 (c), we display a contour plot of C_p for all possible values of x_1 and x_2 (we cut out part of the contour plot corresponding to $\alpha > \tan 7^\circ$). This indicates that there is a clear unique optimum at $x_1/h_0 = 12.3$ and $x_2/h_0 = 24.3$.

For the axisymmetric case we find that the optimal shape has a similar structure and can also be well approximated by parameterisation with x_1 and x_2 . We find that the optimal value of $x_1/h_0 = 6.3$ is a little bit shorter than the two-dimensional case. In fact, we can see in figure 3 (b) and (d) that the shear layer has not reached all the way across the channel by $x = x_1$. Instead, x_1 corresponds to the point where the shear layer reaches the centre of the channel. It reaches the outer wall of the channel slightly further downstream, during the widening section. This could be explained by the fact that pressure gradients due to wall drag are stronger (per unit flux) in the axisymmetric case (e.g. Poiseuille flow (Batchelor 2000)), and therefore the optimal shape cannot afford a longer section of straight, narrow channel. Figure 3 (b, d, f) shows a close comparison between the velocity and pressure in the 2 DOF case and the 100 DOF case. Figure 4 (b) shows the optimum parameter values $x_1/h_0 = 6.3$ and $x_2/h_0 = 19.8$ and the comparison

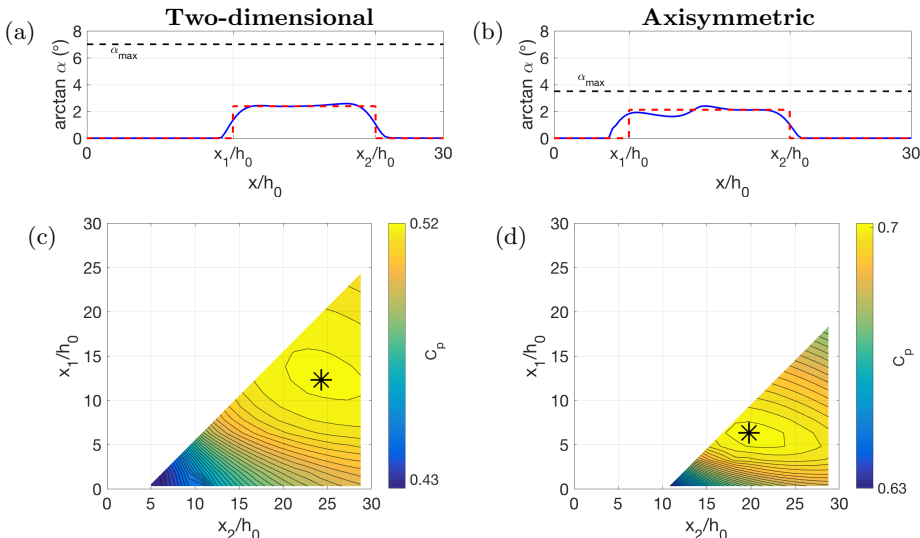


Figure 4: Approximation of the optimal shapes in figure 3 (a, b), where the shape is divided into three sections with divisions at $x = x_1$ and $x = x_2$ (2 degrees of freedom DOF). Two-dimensional case shown in (a, c) and axisymmetric case (b, d). The widening middle section has constant angle given by equation (3.2). (c) Contour plot (taken from (Benham *et al.* 2017)) of pressure recovery C_p (2.10) for all permissible values of x_1 and x_2 such that $\alpha < \alpha_{max} = \tan 7^\circ$. (d) Equivalent plot for axisymmetric case, but with $\alpha_{max} = \tan 3.5^\circ$.

with the control of 100 DOF. The pressure recovery coefficient for 2 DOF is $C_p = 0.6894$ compared to $C_p = 0.7018$ for 100 DOF, suggesting that, as in the two-dimensional case, piecewise linear diffuser shapes are a good approximation.

The contour plot in figure 4 (d) has a larger excluded region because the maximum diffuser angle for axisymmetric flow is $\alpha_{max} = \tan 3.5^\circ$. Nevertheless, the optimum widening angle is around $\alpha \approx \tan 2.1^\circ$, indicating that the upper bound on α is not necessary in this case. The contour plot in figure 4 (d) has a very steep gradient for small values of x_1 , corresponding to situations in which the speed of the slower plug region U_2 becomes zero. As discussed earlier, diffusers have the tendency to accentuate non-uniform flow. From these results we see that this phenomenon is more pronounced in the axisymmetric case, and in fact, the non-uniform flow becomes so accentuated that the slower central plug region stops altogether. This corresponds to a jet-like flow with high kinetic energy flux and, hence, a poor pressure recovery. This is why such steep gradients are observed in the contour plot within this region. We discuss this phenomenon, including an example, in Appendix A.

3.2. Small shear limit

The second case we look at is the limiting case where the flow is almost uniform such that U_1 and U_2 are very similar. The shear between these flows is weak, with a thin shear layer that grows slowly so we denote this case the “small shear limit”. We choose the channel length to be sufficiently short such that the shear layer never reaches across the channel. This case is illustrated in figure 2 (b) and can be compared to the previous, more general, case which is illustrated in figure 2 (a).

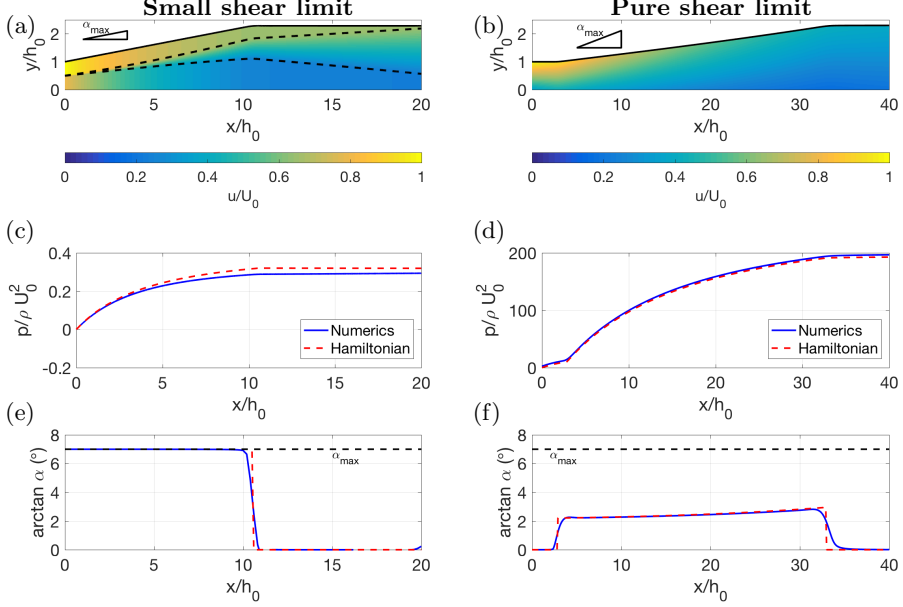


Figure 5: Optimal diffuser shapes, velocity colour maps, pressure plots and diffuser angle plots. (a, c, e) Two-dimensional flow with small shear rate $U_2(0)/U_0 = 0.8$ (near-uniform flow) and short channel length $L/h_0 = 20$ such that the shear layer never reaches across the channel. (b, d, f) Two-dimensional flow where the shear layer has already reached across the channel at the inflow so that there are no plug regions. Inflow velocity ratio is $U_2(0)/U_0 = 0.35$.

For this case, we consider two-dimensional flow and choose parameter values $U_2(0)/U_0 = 0.8$, $h_2(0)/h_0 = 0.5$, $h(L)/h_0 = 2.3$, $L/h_0 = 20$, $\alpha_{min} = 0$ and $\alpha_{max} = \tan 7^\circ$. The other parameters S and f are taken at the same values as the previous cases. We display the optimal shape, velocity colour map and pressure plot in figures 5 (a, c, e). In this case, the optimal shape widens at the maximum angle α_{max} until it reaches the exit width $h(L)$ and then stays straight. Since the shear is small and the flow is almost uniform, there is no risk of accentuating the flow profile drastically. Therefore, wide angles initially are not penalised, allowing the control to take its maximum value. This design is typically what is built in the diffuser industry for uniform inflow (Blevins 1984), where the maximum diffuser angle is set by the limit where boundary layer separation occurs. The optimal control only takes its extremal values, which is sometimes referred to as “bang-bang control”. In section 4.1 we discuss analytical results for this limiting case and prove that the control must be bang-bang.

3.3. Pure shear limit

The final case we investigate is a limiting case in which the shear layer has already spread across the channel, such that $\delta(0) = h(0)$. In this case the flow profile is purely sheared, with no plug regions (see figure 2 (c)). Hence, we call it the “pure shear limit”. We consider two-dimensional flow and choose parameter values $U_2(0)/U_0 = 0.35$, $h_2(0)/h_0 = 0.5$, $h_L/h_0 = 2.3$, $L/h_0 = 40$, $\alpha_{min} = 0^\circ$ and $\alpha_{max} = \tan 7^\circ$. Parameters S and f are taken as the same as before. The optimal channel, velocity map, pressure and control are displayed in figure 5 (b, d, f). The optimal shape is similar to those

in figure 3, with a natural decomposition into two straight sections separated by a widening section. The widening section has an angle that increases from $\alpha \approx \tan 2.5^\circ$ to $\alpha \approx \tan 3^\circ$ and is nowhere greater than $\tan 7^\circ$, showing that the upper bound α was not needed in this case. The optimal shape, like in figure 3, exhibits the balance between the necessity of a straight section that is long enough to allow some mixing, but not too long that wall drag dominates. In this case, which does not involve any of the switching behaviour that occurs when plug regions reach the wall, we derive some analytical results (discussed in section 4.2) which support and help interpret the numerical optimisation. In particular, we investigate the nature of the optimal widening angle which lies in the interval $(\alpha_{min}, \alpha_{max})$. This is of great interest because it indicates that the optimal design is unaffected by the conventional widening angle limit that exists due to boundary layer separation.

4. Analytical results

The numerical optimisation routine outlined in section 3 can be applied to find optimal shapes for any choice of the parameters listed in table 1. We have seen several examples of these in figures 3 and 5. In the two limiting cases displayed in figure 5, the small shear limit and the pure shear limit, it is possible to make some analytical progress which aids our understanding and interpretation of the optimal control. Furthermore, the results discussed in this section include simple relationships that may be of instructive use for the purpose of diffuser design in industry. In both cases we derive a reduced set of equations describing the dynamics, that is amenable to optimal control analysis using Pontryagin's maximum principle (Pontryagin 1987).

4.1. Small shear limit

To start with, we consider a two-dimensional diffuser where the inflow is almost uniform, producing a thin, slowly growing shear layer between the plug flow regions. The channel is sufficiently short that the shear layer never reaches across the channel (see figure 2 (b)). The speed of the plug regions differs by a small amount

$$U_1(0) - U_2(0) = \epsilon V, \quad (4.1)$$

where $\epsilon \ll 1$. If the plug regions always exist, with positive width $h_1 > 0$, $h_2 > 0$, and we assume that the slower flow never stagnates $U_2 > 0$, then we need not consider the complementarity format for Bernoulli's equation. Therefore, we replace equations (2.6) and (2.7) with

$$p + \frac{1}{2}\rho U_i^2 = \frac{1}{2}\rho U_i(0)^2, \quad \text{for } i = 1, 2. \quad (4.2)$$

We consider the distinguished limit where the friction factor f is small such that $f = \epsilon SF$, where $F = O(1)$. For a Reynolds number of $Re = 10^6$ and hydraulically smooth walls, the friction factor is $f = 0.01$. Therefore, if $\epsilon = 0.1$ and $S = 0.11$, then $F = 0.91$. Choosing these parameter values and setting $V/U_1(0) = 2$, we achieve the small shear limit example in figure 5 (a, c, e). We expand variables in powers of the small parameter

ϵ ,

$$U_1 = U_{1_0} + \epsilon \hat{U}_1 + \dots, \quad (4.3)$$

$$U_2 = U_{2_0} + \epsilon \hat{U}_2 + \dots, \quad (4.4)$$

$$h_1 = h_{1_0} + \epsilon \hat{h}_1 + \dots, \quad (4.5)$$

$$h_2 = h_{2_0} + \epsilon \hat{h}_2 + \dots, \quad (4.6)$$

$$p = p_0 + \epsilon \hat{p}_1 + \dots, \quad (4.7)$$

$$\delta = \delta_0 + \epsilon \hat{\delta} + \dots, \quad (4.8)$$

$$\varepsilon_y = \varepsilon_{y_0} + \epsilon \hat{\varepsilon}_y + \dots \quad (4.9)$$

In the limit $\epsilon \rightarrow 0$, equations (2.1)-(2.5) and (4.2) are satisfied by

$$U_{1_0} = U_{2_0} = \frac{U_1(0)h(0)}{h}, \quad (4.10)$$

$$h_{2_0} = h - h_{1_0}, \quad (4.11)$$

$$p_0 = \frac{1}{2} \rho U_1(0)^2 \left(1 - \frac{h(0)^2}{h^2} \right), \quad (4.12)$$

$$\delta_0 = 0, \quad (4.13)$$

$$\varepsilon_{y_0} = \frac{h(0)U_1(0)}{S \int_0^x h(\hat{x}) d\hat{x}}. \quad (4.14)$$

The function h_{1_0} , which represents the location of the centre of the shear layer, is not determined at leading order, but instead at order $O(\epsilon)$. At order $O(\epsilon)$, Bernoulli's equation (4.2) for each plug region is

$$\hat{p} + \rho \hat{U}_1 U_{1_0} = 0, \quad (4.15)$$

$$\hat{p} + \rho \hat{U}_2 U_{1_0} = -\rho U_1(0)V. \quad (4.16)$$

From the relationship $h_1 + h_2 + \delta = h$ at order $O(\epsilon)$, we find that

$$\hat{h}_1 + \hat{h}_2 + \hat{\delta} = 0. \quad (4.17)$$

Thus, the conservation of mass equation (2.3) is

$$\hat{U}_1 h_{1_0} + \hat{U}_2 (h - h_{1_0}) = -V h_2(0), \quad (4.18)$$

and the momentum equation (2.4) is

$$h \frac{d\hat{p}}{dx} + \rho \frac{d}{dx} \left(2U_{1_0} \hat{U}_1 h_{1_0} + 2U_{1_0} \hat{U}_2 (h - h_{1_0}) \right) = -\frac{1}{8} S F \rho U_{1_0}^2. \quad (4.19)$$

Thus, using equations (4.15) - (4.17), we can simplify equation (4.19) to an equation purely involving h_{1_0} and h

$$V h^2 \frac{dh_{1_0}}{dx} - V h h_{1_0} \frac{dh}{dx} = -\frac{1}{8} F S h(0)^2 U_1(0). \quad (4.20)$$

Equation (4.20) has solution

$$h_{1_0} = h \left(\frac{h_1(0)}{h(0)} - \int_0^x \frac{S F h(0)^2 U_1(0)}{8 V h(\hat{x})^3} d\hat{x} \right), \quad (4.21)$$

which we can insert into the momentum equation to produce a differential equation for the pressure correction \hat{p} in terms of the channel shape and its derivative $\alpha = h'(x)$,

$$\frac{d\hat{p}}{dx} = -\frac{\rho U_1(0)^2 h(0)^2}{h^3} \left(\frac{2V}{U_1(0)} \left(1 - \frac{h_1(0)}{h(0)} \right) \alpha + \frac{SF}{8} \right). \quad (4.22)$$

We now solve the optimal control problem outlined in section 2.2. Since the inflow conditions are fixed and we take $p(0) = 0$, maximising C_p is equivalent to maximising pressure at the outlet $p(L)$. Furthermore, the constraint equations have been reduced to (4.22). Therefore the optimal control problem, including terms up to and including order $O(\epsilon)$, and written as a system of first order differential equations, is as follows:

$$\max_{\alpha_{min} \leq \alpha(x) \leq \alpha_{max}} \Phi := p(L), \quad (4.23)$$

such that

$$\frac{dp}{dx} = \frac{\rho U_1(0)^2 h_0^2}{h^3} \left(\left(1 - \epsilon \frac{2V}{U_1(0)} \left(1 - \frac{h_1(0)}{h_0} \right) \right) \alpha - \epsilon \frac{SF}{8} \right), \quad (4.24)$$

$$\frac{dh}{dx} = \alpha, \quad (4.25)$$

$$h(0) = h_0, \quad (4.26)$$

$$p(0) = 0, \quad (4.27)$$

$$h(L) = h_L. \quad (4.28)$$

We now solve this reduced problem using Pontryagin's maximum principle (Pontryagin 1987). The Hamiltonian for this system is

$$H = \lambda_p \frac{dp}{dx} + \lambda_h \frac{dh}{dx}, \quad (4.29)$$

where λ_p and λ_h are the adjoint variables which satisfy the adjoint equations

$$\frac{d\lambda_p}{dx} = -\frac{\partial H}{\partial p}, \quad (4.30)$$

$$\frac{d\lambda_h}{dx} = -\frac{\partial H}{\partial h}. \quad (4.31)$$

According to Pontryagin's maximum principle, variables which appear in the objective function evaluated at $x = L$ must have natural boundary conditions which apply to their corresponding adjoint variables (Pontryagin 1987). Since the objective function only depends on pressure at the outlet $\Phi = p(L)$, we have the natural boundary condition

$$\lambda_p(L) = \frac{\partial \Phi}{\partial p} = 1. \quad (4.32)$$

Considering equation (4.32) and the fact that there is no dependance of the Hamiltonian (4.29) on the pressure p , equation (4.30) tells us that $\lambda_p = 1$ for all values of x . There is no natural boundary condition for λ_h since we are enforcing a condition on h at the outlet $x = L$. The last condition from Pontryagin's maximum principle is the optimality condition, which usually takes the form $\partial H / \partial \alpha = 0$. However, following Pitcher (2009) and McDanell & Powers (1971), since the Hamiltonian is linear in the control α , the

optimality condition takes the form

$$\alpha(x) = \begin{cases} \alpha_{max}, & \text{if } H_\alpha > 0, \\ \in [\alpha_{min}, \alpha_{max}], & \text{if } H_\alpha = 0, \\ \alpha_{min}, & \text{if } H_\alpha < 0, \end{cases} \quad (4.33)$$

where we have introduced the shorthand notation $H_\alpha = \partial H / \partial \alpha$. If H_α is only zero at single values of x , the control is said to be “bang-bang”. If the Hamiltonian satisfies $H_\alpha = 0$ and $dH_\alpha/dx = 0$ for a finite interval, then the control is said to have a “singular arc”. However, upon close inspection, we see that

$$\frac{dH_\alpha}{dx} = -\frac{3\epsilon\rho SFU_1(0)^2 h(0)^2}{8h^4}, \quad (4.34)$$

which is negative for all values of x . Hence, it is impossible for singular arcs to exist in this case. Therefore the control is bang-bang with

$$\alpha(x) = \begin{cases} \alpha_{max}, & \text{for } x \in [0, \gamma], \\ \alpha_{min}, & \text{for } x \in [\gamma, L], \end{cases} \quad (4.35)$$

where the switching point γ is given by

$$\gamma = \frac{h_L - h_0 - \alpha_{min}L}{\alpha_{max} - \alpha_{min}}. \quad (4.36)$$

In figures 5 (c, e), we plot the solution to the optimal control problem found using the Hamiltonian approach on top of the solution found using the numerical optimisation routine outlined in section 3. It is clear that the numerical optimisation routine has correctly found the bang-bang control which we have derived here, with $\gamma/h_0 = 10.59$ (the small discrepancy is probably due to the finite value of ϵ).

It should be noted that the adjoint variable λ_h is only solved for up to a constant of integration C (from integrating equation (4.31)) since it has no boundary condition. Instead, C is determined by the condition that $H_\alpha(\gamma) = 0$ for some $\gamma \in (0, L)$. However, in the case where we also allow the channel length L to be a control as well as α , according to Pontryagin’s maximum principle (Pitcher 2009; Pontryagin 1987), we have the additional constraint on the Hamiltonian at the final point

$$H(L) = 0. \quad (4.37)$$

Using (4.35), we can integrate the system (4.24)-(4.32) up to the constant of integration C , which is determined by

$$H(L) = C = 0. \quad (4.38)$$

This is inconsistent with the switching point condition $H_\alpha(\gamma) = 0$ mentioned above (i.e. the two conditions would overdetermine the constant C). We therefore conclude that there is no switching point (i.e. $\gamma = 0$ or L), so that $H_\alpha \neq 0, \forall x \in [0, L]$. For the case in figure 5 (a, c, e), it is clear that $L = 0$ is impossible, so we conclude that the optimal diffuser length is $L = \gamma$. Therefore, including L as a control and taking $\alpha_{min} = 0^\circ$, the optimal diffuser shape for the small shear limit is one which expands at the maximum angle until h reaches h_L , at which point the channel terminates.

4.2. Pure shear limit

The next limiting case we investigate is the pure shear limit, in which the shear layer has already reached across the channel at the inflow, such that there are no plug regions

(see figure 2 (c)). Since $h_1 = h_2 = 0$ and $\delta = h$, the velocity profile, given by equation (2.1), reduces to

$$u = U_2 + (U_1 - U_2)\frac{y}{h}. \quad (4.39)$$

Conservation of mass and momentum equations (2.3), (2.4) reduce to

$$\frac{h}{2}(U_1 + U_2) = Q, \quad (4.40)$$

$$h\frac{dp}{dx} + \frac{1}{3}\rho\frac{d}{dx}(h(U_1^2 + U_1U_2 + U_2^2)) = -\frac{1}{8}\rho fU_1^2. \quad (4.41)$$

It is convenient to introduce two new variables, the velocity difference between maximum and minimum velocities $\tilde{U} = U_1 - U_2$ and the average velocity $\bar{U} = (U_1 + U_2)/2$. In terms of these variables, the shear rate is

$$\varepsilon_y = \frac{\tilde{U}}{h}, \quad (4.42)$$

and hence equation (2.2) becomes

$$\frac{d\tilde{U}}{dx} - \frac{\tilde{U}}{h}\frac{dh}{dx} = -\frac{S\tilde{U}^2}{\bar{U}h}. \quad (4.43)$$

Re-writing equations (4.40) and (4.41) in terms of the new variables, we get

$$\bar{U}h = Q, \quad (4.44)$$

$$\frac{dp}{dx} = \frac{\rho}{h} \left(-\frac{f}{32}(2\bar{U} + \tilde{U})^2 - \frac{1}{12}\frac{d}{dx} \left(h(12\bar{U}^2 + \tilde{U}^2) \right) \right). \quad (4.45)$$

We now solve the optimal control problem outlined in section 2.2. As in section 4.1 we maximise pressure at the outlet $p(L)$. Furthermore, the constraint equations have been reduced to (4.43) and (4.45). We formulate the optimal control problem in terms of \tilde{U} , p , and h by substituting $\bar{U} = Q/h$ and $\frac{dh}{dx} = \alpha$ into (4.43) and (4.45). Therefore, the optimal control problem is as follows:

$$\max_{\alpha_{min} \leq \alpha(x) \leq \alpha_{max}} \Phi := p(L), \quad (4.46)$$

such that

$$\frac{d\tilde{U}}{dx} = \frac{\tilde{U}}{h}\alpha - \frac{S\tilde{U}^2}{Q}, \quad (4.47)$$

$$\frac{dp}{dx} = \frac{\rho(-12fQ^3 - 12fQ^2q - 3fQq^2 + 16Sq^3 + \alpha(96Q^3 - 24Qq^2))}{96Qh^3}, \quad (4.48)$$

$$\frac{dh}{dx} = \alpha, \quad (4.49)$$

$$p(0) = 0, \quad (4.50)$$

$$h(0) = h_0, \quad (4.51)$$

$$h(L) = h_L, \quad (4.52)$$

where we have introduced the new variable $q = h\tilde{U}$ as a shorthand notation. Similarly to section 4.1, the Hamiltonian for the system is constructed as

$$H = \lambda_{\tilde{U}}\frac{d\tilde{U}}{dx} + \lambda_p\frac{dp}{dx} + \lambda_h\frac{dh}{dx}, \quad (4.53)$$

which is linear in the control α . The adjoint equations are

$$\frac{d\lambda_{\tilde{U}}}{dx} = -\frac{\partial H}{\partial \lambda_{\tilde{U}}}, \quad (4.54)$$

$$\frac{d\lambda_p}{dx} = -\frac{\partial H}{\partial p}, \quad (4.55)$$

$$\frac{d\lambda_h}{dx} = -\frac{\partial H}{\partial h}, \quad (4.56)$$

which have the natural boundary conditions

$$\lambda_{\tilde{U}}(L) = \frac{\partial \Phi}{\partial \tilde{U}} = 0, \quad (4.57)$$

$$\lambda_p(L) = \frac{\partial \Phi}{\partial p} = 1. \quad (4.58)$$

There is no natural boundary condition for λ_h since h is already prescribed at $x = L$. Finally, as in section 4.1, the optimality condition is (4.33). In order for there to be a singular arc, we must have $H_\alpha = 0$ and $dH_\alpha/dx = 0$ for a finite interval. Following Pitcher (2009) and McDanell & Powers (1971), in this interval the value of the control is given by $\alpha = \alpha^*$, where α^* is defined by

$$\frac{d^2 H_\alpha}{dx^2}(\alpha^*) = 0. \quad (4.59)$$

Setting $H_\alpha = dH_\alpha/dx = 0$, and using equation (4.59), we find that there will only be a singular arc when

$$\alpha^* = \frac{Sq^2(-fQ^2 + 2Sq^2)}{6fQ^4 + fQ^3q + 2Q Sq^3} \quad \text{for } x \in [x_1, x_2], \quad (4.60)$$

for some $x_2 > x_1$. Thus, (4.33) becomes

$$\alpha(x) = \begin{cases} \alpha_{max}, & \text{if } H_\alpha > 0, \\ \alpha^*, & \text{if } H_\alpha = 0, \\ \alpha_{min}, & \text{if } H_\alpha < 0, \end{cases} \quad (4.61)$$

and we can solve the coupled system (4.47)-(4.61) numerically for the optimal control and corresponding solution. In certain cases, where the singular arc value α^* is constant, we find analytical solutions, which we discuss at the end of this section.

In figure 5 (b, d, f) we plot the solution to the optimal control problem found using the Hamiltonian approach over the solution found using the numerical optimisation routine outlined in section 3. It is clear that both approaches have found the same solution. The singular arc represents the balance between mixing and widening effects in the diffuser. It is necessary to mix the non-uniform flow before widening it because widening tends to accentuate the non-uniform profile, producing a high-kinetic energy low-pressure outlet. Therefore, the control initially takes its minimum value $\alpha = 0^\circ$. However, a straight section which is too long is detrimental to pressure recovery because of wall drag. Hence a widening section is required after a certain critical length. The optimum value of α in the widening section represents a balance between mixing and widening the flow. If α is too large, then the flow profile will become too non-uniform at the outlet. Conversely, if α is too shallow, the pressure at the outlet will be too low due to wall drag losses. The singular arc is interesting from both a mathematical point of view, but also from an engineering point of view. It clearly shows that diffuser designs for non-uniform inflow should take

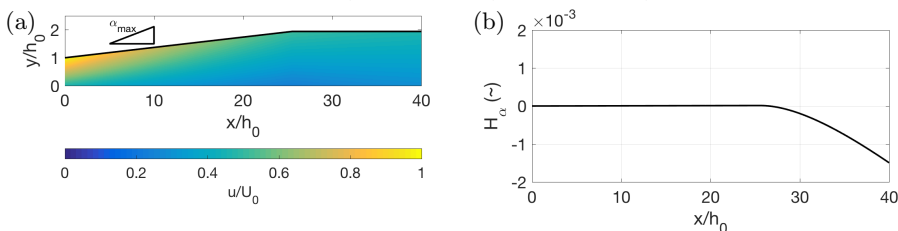


Figure 6: Constant singular arc solution displaying velocity colour map and a plot of $H_\alpha = \partial H / \partial \alpha$, where the Hamiltonian H is given by (4.53), for parameter values $S = 0.11$ and $f = 0.01$. The inflow velocity ratio $U(0) = 0.471$ is given by (4.64) and the singular arc value $\alpha^* = \tan 2.26^\circ$ is given by (4.65).

into account the nature of the non-uniform inflow profile. The optimum widening angle for manufacture is given by equation (4.60). Unfortunately, equation (4.60) is difficult to calculate in general (q is a variable), but we find that for certain parameter values, it takes a simpler and more useful form.

In general, the value of α during the singular arc is not constant, yet in certain cases, such as figure 4 (b), it doesn't vary much over the singular arc interval. This raises the question of whether it is possible to find constant α solutions. Noticing how the only variable in equation (4.60) is $q = h\tilde{U}$, we seek solutions with constant q . Furthermore, we restrict our attention to solutions which begin on the singular arc. From equation (4.47), we see that constant α^* solutions only exist if

$$\alpha^* = \frac{Sq}{2Q}. \quad (4.62)$$

Therefore, reconciling equations (4.60) and (4.62), it can be shown that constant singular arc solutions exist for parameters which satisfy

$$qQ^3S \left(-3f \left(\frac{q}{Q} + 2 \right) + 2 \frac{q^3}{Q} S \right) = 0. \quad (4.63)$$

Excluding $q = 0$ and $Q = 0$, and assuming that f and S are fixed, we are left with solving equation (4.63) for q/Q . Substituting $U_1(0)$, $U_2(0)$ and $h(0)$ back into (4.63), we rewrite the equation in terms of the inlet velocity ratio $U(0) = U_2(0)/U_1(0)$, giving

$$4S(-1 + U(0))^3 + 3f(1 + U(0))^2 = 0. \quad (4.64)$$

Similarly, (4.62) becomes

$$\alpha^* = S \left(\frac{1 - U(0)}{1 + U(0)} \right). \quad (4.65)$$

Ignoring imaginary solutions, there is one solution $U(0)$ which satisfies equation (4.64). We also need to ensure that both $H_\alpha = 0$ and $dH_\alpha/dx = 0$ for all values of x . This will enforce further constraints on the other parameters of the problem (e.g. h_L/h_0 and L/h_0), which we do not discuss here. As an example of such a constant singular arc solution, we choose parameter values $S = 0.11$ and $f = 0.01$ (which are equivalent to the examples in figures 3 and 5), from which, using equations (4.64) and (4.65), we have an inflow velocity ratio $U(0) = 0.471$ and a singular arc value of $\alpha^* = \tan 2.26^\circ$. We find that $H_\alpha = 0$ and $dH_\alpha/dx = 0$ along the singular arc if we choose the remaining parameter values $h_L/h_0 = 1.94$ and $L/h_0 = 40$. In figure 6 we display the velocity colour map for this solution, together with a plot of H_α . Clearly we see that the solution starts

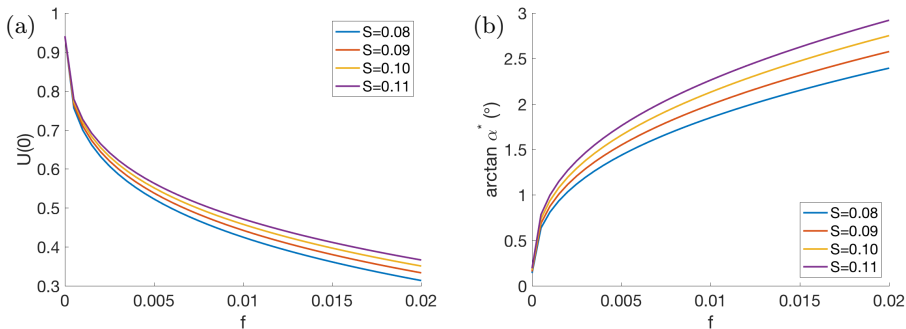


Figure 7: Parameter analysis for the constant α^* singular arc solution. (a) The constant singular arc solution only exists for a certain value of $U(0) = U_2(0)/U_1(0)$, given by equation (4.64), which is a function of the parameters S and f . (b) The constant value of α^* on the singular arc, given by (4.65), also depends on S and f .

on the singular arc until the expansion ratio $h_L/h_0 = 1.94$ is reached, at which point H_α becomes negative, such that the remaining length of the diffuser has angle $\alpha_{min} = 0^\circ$.

It is of further interest to investigate how the singular arc depends on the model parameters f and S . We plot the relationship between these parameters, and both the inflow velocity ratio $U(0)$, which satisfies (4.64), and constant singular arc value α^* (4.65) in figure 7. It is clear that increasing the friction factor f results in a higher α^* . This is to be expected, since larger wall drag will penalise smaller angles more. Increasing the spreading parameter S also increases α^* . This is because higher spreading rates results in better mixing, and hence, wider angles are more affordable. For the inlet velocity ratio $U(0)$, we see a decrease with friction factor and an increase with spreading rate. We do not have a physical interpretation for these effects, but they represent the necessary conditions for a constant singular arc solution to exist and commence at $x = 0$. For other inlet velocity ratios it may still be possible to have constant α^* solutions that start further down the channel, similar to the example in figure 5 (b).

5. Comparison with results from a k - ϵ model

In this section we discuss comparisons between the optimal shapes found using the mathematical model in the previous sections to calculations from CFD. In Benham *et al.* (2017) there are comparisons between the mathematical model and a k - ϵ turbulence model (Launder & Spalding 1974), as well as experimental data generated with Particle Image Velocimetry (PIV). Here we use the same k - ϵ model to compare with some of the optimisation results. Moreover, since a thorough comparison between the mathematical model and CFD has already been discussed in (Benham *et al.* 2017), we do not perform comparisons for all of the optimisation results of section 3. Instead we look at the geometry in figure 5 (a) as a single example.

Consider the example in figure 5 (a), as discussed in section 4.1. In order to compare with the mathematical model we use precisely the same inlet velocity profile in the CFD. Inlet conditions for the turbulence variables k and ϵ are given by the free-stream boundary conditions (Schlichting *et al.* 1960) $k = I^2 \times 3/2 (u^2 + v^2)$ and $\epsilon = 0.09k^{3/2}/\ell$, with turbulence intensity $I = 10\%$ and mixing length $\ell = 0.1h_0$ (10% of the channel width).

In figures 8 (a, b) we display colour plots of the time-averaged streamwise velocity u

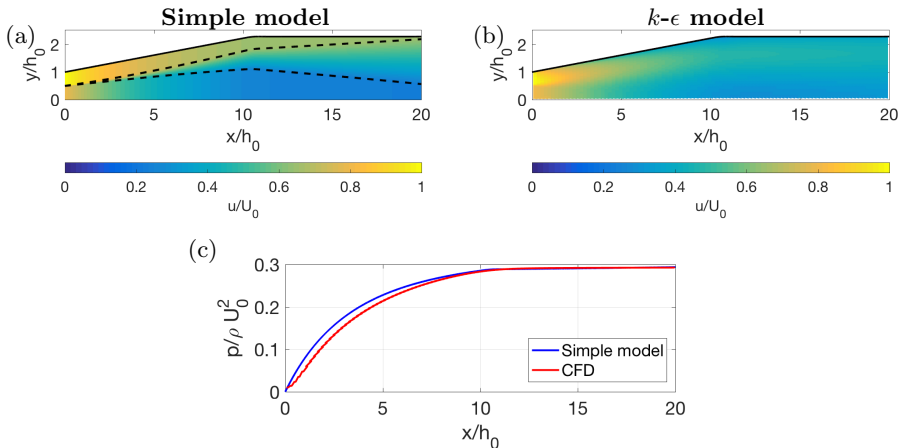


Figure 8: Comparison between mathematical model and CFD for the optimal shape in figure 5 (a). (a, b) Time-averaged velocity in the x direction, u , where in the case of the mathematical model, (a), we also overlay dashed lines indicating the width of the shear layer. (c) Time-averaged pressure profile (averaged across the width of the channel).

generated with both the simple model and the k - ϵ model. There is a good comparison between the two, with the mathematical model capturing the dominant features of the flow, such as maximum and minimum velocities, and the width of the shear layer. We compare the time-averaged pressure calculated with the k - ϵ model, averaged across the width of the channel, to the pressure predicted by our model in figure 8 (c), and we find that they agree well.

In section 3, we investigated reducing the dimension of the control α by splitting it into three piecewise constant sections divided by x_1 and x_2 , which we treated as free parameters. Here we make the same simplification, reducing the degrees of freedom of the control to 2, and we explore the parameter space generated by x_1 and x_2 , using CFD to calculate pressure recovery. Each calculation made by the CFD is much more computationally expensive than that of the simple model, but because of the low dimension of the degrees of freedom, we can still feasibly explore the different possible combinations of x_1 and x_2 . This would not be tractable, however, if we were to use 100 degrees of freedom, as we did with the simple model in section 3.

In figure 9 we plot contours of pressure recovery C_p , given by equation (2.10), as a function of the two parameters x_1 and x_2 , where C_p is calculated using CFD instead of the simplified model, as in figure 4. Similarly to the contour plots in figure 4, we exclude values of x_1 and x_2 which result in a diffuser angle larger than $\tan 7^\circ$ for the two-dimensional case and $\tan 3.5^\circ$ for the axisymmetric case.

Comparing figures 4 and 9, we see that the optimum diffuser shape using both the simple model and CFD, is characterised by similar values of x_1 and x_2 . In the two-dimensional case, according to CFD, the optimum diffuser shape has $x_1/h_0 = 11$ and $x_2/h_0 = 25$, with a pressure recovery of $C_p = 0.55$. According to the simplified model, the optimum diffuser shape has $x_1/h_0 = 12.3$ and $x_2/h_0 = 24.3$, with a pressure recovery of $C_p = 0.52$, which is surprisingly close to that obtained with CFD. Similarly, for the axisymmetric case, CFD suggests an optimum diffuser shape with $x_1/h_0 = 7$ and $x_2/h_0 = 21$, giving a pressure recovery of $C_p = 0.73$, whereas the simplified model suggests $x_1/h_0 = 6.3$ and $x_2/h_0 = 19.8$, with a pressure recovery of $C_p = 0.70$. These

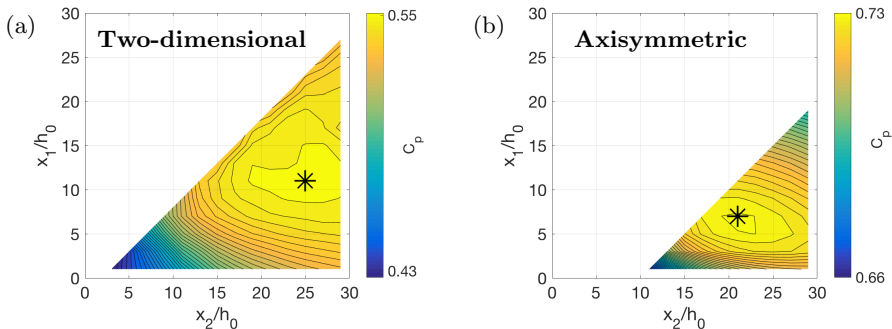


Figure 9: Contour plots of pressure recovery C_p , given by (2.10), over all permissible values of x_1 and x_2 , calculated using the k - ϵ model ((a) taken from (Benham *et al.* 2017)). Direct comparison is made with figure 4, where the same contour plots are calculated using the simple model.

results indicate that the optimal shapes found using the numerical optimisation routine and the simplified model are similar to the optimal shapes that would be found if we were to use the k - ϵ turbulence model as a forward model. Hence, this gives us confidence that the optimal shapes generated using the simplified model are close to true optimal shapes in reality.

6. Discussion and conclusion

Although we have investigated optimum diffuser shapes in a number of specific cases, we have not yet explored the various parameters of the model thoroughly. In table 1 we list the parameters of the model. We now briefly discuss the effect that each of these parameters has on the optimal shapes, though, since there are many parameters, we do not provide plots for the analysis of every single parameter.

One of the most important parameters is the velocity ratio $U_2(0)/U_0$ of the inflow. To explore this parameter, we investigate optimal diffuser shapes for a fixed inflow with $h_2(0)/h_0 = 0.5$, an expansion ratio $h_L/h_0 = 2.3$ and a length ratio $L/h_0 = 40$, and we vary the velocity ratio. The results of the optimisation are displayed in figure 10, for $U_2(0)/U_0 = 0.3$ and $U_2(0)/U_0 = 0.7$. We see that the effect of a larger velocity ratio is that an initial widening section becomes favourable. This is because when the inflow is more uniform, wider angles penalise pressure recovery less. Therefore, the balance is tipped in favour of reducing wall drag by expanding the channel a little. In the extreme case where $U_2(0)/U_0$ becomes close to unity, we have seen in section 4.1 that this initial widening section dominates throughout, such that the optimal control is purely bang-bang, with no singular arc. Notice how in the case of large velocity ratio the shape can no longer be approximated with the parameterisation of x_1 and x_2 .

The effect of increasing or decreasing the ratio of the size of the plug regions from $h_2(0)/h_0 = 0.5$ is that the distance it takes for one of the plug regions to disappear becomes smaller. If the velocity ratio is small then, as described earlier, this distance is critical because it marks the point where the flow is sufficiently mixed that it is acceptable to expand thereafter at a wider angle. Hence, the effect of increasing or decreasing $h_2(0)/h_0$ is that this critical distance becomes smaller.

The effects of varying the diffuser expansion ratio h_L/h_0 and length ratio L/h_0 are more obvious and less interesting. Neither of them affect the optimum widening angle,

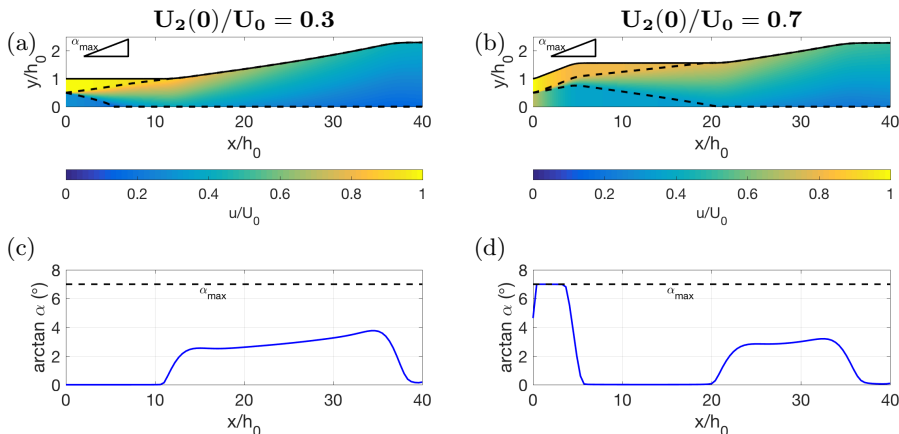


Figure 10: Investigation of the dependence of optimal diffuser shapes on the inflow velocity ratio in the two-dimensional case, showing velocity colour maps (a, b) and plots of the control α (c, d). In both cases we choose an inflow with $h_2(0)/h_0 = 0.5$, an expansion ratio $h_L/h_0 = 2.3$ and a length ratio $L/h_0 = 40$. The lower limit for the diffuser angle in both cases is $\alpha_{min} = 0^\circ$. The upper limit is $\alpha_{max} = \tan 7^\circ$.

but instead simply make the diffuser continue to expand wider and longer respectively. This is because they don't affect the crucial balance between wall drag and mixing effects.

Varying the upper and lower bounds on the diffuser angle, α_{max} and α_{min} , only affects the optimal solution if the diffuser angle touches the bounds over an interval. For example, in figure 10 (a, c) we see that α never touches α_{max} . Therefore, in this case, raising α_{max} would have no effect on the solution. However, α clearly lies on the lower bound α_{min} over an interval at the beginning and near the end of the domain. Therefore, varying α_{min} here moves the optimal control along with it.

Although, for the most part it is not possible to alter the parameters S and f , it is of interest to understand their effect on the optimal diffuser shape. For example, a larger value of the spreading parameter S is associated with a larger shear layer growth rate. For larger S , the shear layer will entrain the plug regions over a shorter distance. Similarly to varying $h_2(0)/h_0$, this decreases the critical distance after which expansion occurs. We have already discussed the effect of S on the singular arc in section 4.2.

For rougher channels with a larger Darcy friction factor f , thinner channels and smaller angles will be penalised more. In such cases, the optimum widening angle is larger. Furthermore, if f is sufficiently large, it becomes more advantageous to have an initial widening section, similar to situations where the velocity ratio $U_2(0)/U_0$ is large. In the extreme case where wall drag dominates, the control becomes bang-bang because the penalty of worsening the non-uniform flow is eclipsed by the effect of wall drag. For very small wall drag, the optimal diffuser shape appears to prioritise mixing over widening the flow. In these cases, thin channels and small diffuser angles are not penalised very much, such that the critical distance after which expansion occurs is precisely the point where the shear layer has reached across the entire channel. At this point the flow is sufficiently mixed and can afford expansion.

To conclude, we have developed a numerical optimisation routine to find the diffuser shape which maximises pressure recovery for given non-uniform inflow, in both two-dimensional and axisymmetric cases. The optimisation uses a simplified mathematical model for the development of turbulent shear layers in confining channels. We find that

some of the optimal diffuser shapes are well approximated by shapes which are composed of two straight sections separated by a widening section with a constant widening angle. The optimum widening angle is less than the angle at which boundary layer separation typically occurs, suggesting that the effects of non-uniform inflow are more critical to performance when it comes to diffuser design.

In two limiting cases we use analytical techniques to interpret the optimal diffuser shapes found with the numerical optimisation. The first of these cases is the small shear limit, where the inflow is almost uniform, in which case the optimal control is bang-bang, such that the diffuser widens at the maximum possible angle until it reaches the desired cross-sectional area, and then remains at that area. The second case is the pure shear limit, where the inflow is a purely sheared flow with no plug regions. In this case, the optimal control may have a singular arc where, on an interval, the diffuser angle takes values between its upper and lower bounds. We show that in certain cases the singular arc corresponds to a constant angle and this angle depends on the friction factor f and the spreading parameter S . We compare some of the numerical optimisation results with CFD simulations using a k - ϵ turbulence model, finding good agreement. In the case where we approximate the diffuser shape with piecewise linear sections, we show that both the simplified model and the CFD share almost identical optimal shapes. This suggests that the optimal shapes found using the numerical optimisation and the simplified model are indeed close to the true optimal shapes in reality.

This publication is based on work supported by the EPSRC Centre for Doctoral Training in Industrially Focused Mathematical Modelling (EP/L015803/1) in collaboration with VerdErg Renewable Energy Limited and inspired by their novel Venturi-Enhanced Turbine Technology for low-head hydropower.

Appendix A.

We have discussed how diffusers have the tendency to accentuate non-uniform flow. In extreme cases, where the diffuser angle is too large, it is possible for regions of the flow to slow to zero velocity and recirculate. Let us now consider diffusers which have a non-uniform inflow velocity given by (2.1). In our mathematical model, outlined in section 2.1, we account for the possibility of a stagnated region by introducing the velocity of the slower plug region U_2 into Bernoulli's equation (2.7) in the form of a complementarity condition. In this way, if the slower central plug region reaches zero velocity, we model this as a region of dead water and maintain it at zero velocity. In reality these regions have relatively slow recirculation. We do not resolve the recirculation, but instead we resolve the size of the regions and treat them as having average streamwise velocity $u = 0$. In order to justify this model assumption we compare it with CFD calculations for a diffuser with a stagnated region.

To make the comparison, we choose an inflow velocity with $U_2(0)/U_0 = 0.75$ and $h_2(0)/h_0 = 0.5$. We choose a relatively large value of $U_2(0)/U_0$ to show that stagnation can occur for even moderately non-uniform inflow conditions. The diffuser that we select has constant widening angle $\alpha = \tan 11^\circ$ and has non-dimensional length $L/h(0) = 30$. For the CFD, we use the same k - ϵ turbulence model as in section 5. In figure 11 we compare the results of the model and the CFD. Time-averaged velocity colour maps are compared in figures 11 (a, b), where we indicate the stagnated region in our model (a) with a red contour. The comparison is good, with the model capturing the dominant flow features, such as the width of the shear layer. In figure 11 (c) we display streamlines

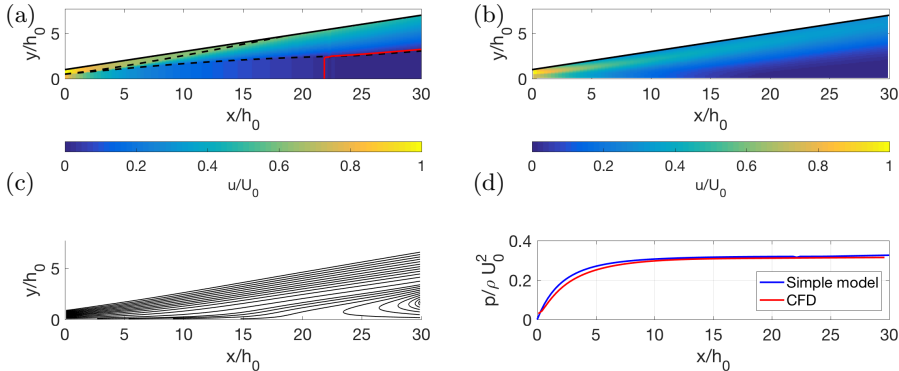


Figure 11: Comparison between mathematical model and CFD for a two-dimensional diffuser with a stagnation region in the centre. (a, b) Time-averaged velocity u colour maps, where, in the case of the mathematical model (a), we overlay black dashed lines to indicate the shear layer, and a red contour to indicate the stagnated zone. (c) Streamlines calculated from CFD. (d) Time-averaged pressure profile averaged across the width of the channel. We use an inflow velocity with $U_2(0)/U_0 = 0.75$, $h_2(0)/h_0 = 0.5$ and a diffuser angle of $\alpha = \tan 11^\circ$.

calculated using CFD. These indicate that there is indeed a stagnated region with recirculation in the centre of the diffuser. This region is located in approximately the same position, and has approximately the same size as the prediction from the mathematical model. The time-averaged pressure profile, averaged across the channel width is plotted in figure 11 (d) and, again, it shows good agreement between the CFD and our model, suggesting that our model accurately captures the general behaviour of the diffuser when it has a stagnated region.

REFERENCES

- BATCHELOR, GK 2000 *An introduction to fluid dynamics*. Cambridge University Press.
- BENHAM, GP, CASTREJON-PITA, AA, HEWITT, IJ, PLEASE, CP, STYLE, RW & BIRD, P 2017 Turbulent shear layers in confining channels. *arXiv preprint arXiv:1705.01046*.
- BEZANSON, J, EDELMAN, A, KARPINSKI, S & SHAH, VB 2017 Julia: A fresh approach to numerical computing. *SIAM Review* **59** (1), 65–98.
- BLEVINS, RD 1984 Applied fluid dynamics handbook. New York, Van Nostrand Reinhold Co., 1984, 568 p. **1**.
- CHAMORRO, LP, HILL, C, MORTON, S, ELLIS, C, ARNDT, REA & SOTIROPOULOS, F 2013 On the interaction between a turbulent open channel flow and an axial-flow turbine. *J. Fluid Mech.* **716**, 658–670.
- DOUGLAS, JF, GASIOREK, JM & SWAFFIELD, JA 1979 *Fluid Mechanics*. Pitman.
- DUNNING, I, HUCHETTE, J & LUBIN, M 2017 Jump: A modeling language for mathematical optimization. *SIAM Review* **59** (2), 295–320.
- FILIPENCO, VG, DENIZ, S, JOHNSTON, JM, GREITZER, EM & CUMPSTY, NA 1998 Effects of inlet flow field conditions on the performance of centrifugal compressor diffusers: Part idiscrete-passage diffuser. *ASME J. Turbomach* **122**, 1–10.
- GUNZBURGER, MD 2002 *Perspectives in flow control and optimization*. SIAM.
- JONES, MA & SMITH, FT 2003 Fluid motion for car undertrays in ground effect. *Journal of engineering mathematics* **45** (3-4), 309–334.
- KANG, S, YANG, X & SOTIROPOULOS, F 2014 On the onset of wake meandering for an axial flow turbine in a turbulent open channel flow. *J. Fluid Mech.* **744**, 376–403.

- LAUNDER, BE & SPALDING, DB 1974 The numerical computation of turbulent flows. *Computer Methods in Applied Mechanics and Engineering* **3** (2), 269–289.
- MCDANELL, JP & POWERS, WF 1971 Necessary conditions joining optimal singular and nonsingular subarcs. *SIAM Journal on Control* **9** (2), 161–173.
- MCKEON, BJ, ZAGAROLA, MV & SMITS, AJ 2005 A new friction factor relationship for fully developed pipe flow. *J. Fluid Mech.* **538**, 429.
- NOCEDAL, J & WRIGHT, SJ 2006 Numerical optimization, second edition.
- PITCHER, AB 2009 Mathematical modelling and optimal control of constrained systems. PhD thesis, University of Oxford.
- PONTRYAGIN, LS 1987 *Mathematical theory of optimal processes*. CRC Press.
- SCHLICHTING, H, GERSTEN, K, KRAUSE, E, OERTEL, H & MAYES, K 1960 *Boundary-layer theory*, , vol. 7. Springer.
- SIMONE, S, MONTOMOLI, F, MARTELLI, F, CHANA, KS, QURESHI, I & POVEY, T 2012 Analysis on the effect of a nonuniform inlet profile on heat transfer and fluid flow in turbine stages. *Journal of Turbomachinery* **134** (1), 011012.
- WÄCHTER, A & BIEGLER, LT 2006 On the implementation of an interior-point filter line-search algorithm for large-scale nonlinear programming. *Mathematical programming* **106** (1), 25–57.